High-Gain Antipodal Vivaldi Antenna With Pseudoelement and Notched Tapered Slot Operating at (2.5 to 57) GHz

Jack Eichenberger, Ersin Yetisir, *Member, IEEE*, and Nima Ghalichechian, *Senior Member, IEEE*

***Abstract*— Novel methods of improving directivity and decreasing sidelobe radiation via the addition of an elliptical pseudoelement and irregularly spaced notches in the tapered slot antenna are presented in this paper. This antenna has been shown to be functional over the C, X, K_u, K, K_a, and portions of the *S*- and *V*-bands covering (2.5 to 57) GHz (22.8:1 bandwidth, defined where VSWR < 3). Minimum and maximum realized gains of 4 and 16 dB were achieved at 2.7 GHz and 29.8 GHz, respectively. The antenna offers directive radiation patterns with a half-power beamwidth under 40° for frequencies above 6 GHz and under 30° for frequencies above 32 GHz. As compared with other Vivaldi antennas reported in the past, the proposed design offers a larger bandwidth while providing higher peak gain and average gain. Good agreement was observed between simulation and measurements.**

***Index Terms*— Notched, pseudoelement, tapered slot antenna, ultra-wideband (UWB), Vivaldi antenna.**

I. Introduction

ULTRA-WIDEBAND (UWB) antennas have numerous advantages compared to their narrow-band counterparts. They can significantly reduce the footprint of a system by replacing multiple antennas traditionally needed to cover numerous bands. In an imaging system, the image quality can be improved since a wider band corresponds to higher information content. For defense applications, the UWB communication is desirable, as the system can continue to function when a specific frequency band is jammed.

A tapered slot antenna or Vivaldi is a natural choice for this application, as it offers wideband performance with a modest footprint. The Vivaldi was originally proposed by Gibson [1] in 1979. The tapered slot was coplanar, but an antipodal extension of this design was given by Gazit [2] in 1988. The antipodal Vivaldi antenna lends itself well to a microstrip to parallel stripline transition, allowing for a simple feeding structure that can support the UWB operation. A balanced antipodal Vivaldi antenna, in which a third conductive layer is added to remove E-field skew, may be used in cases, where high cross-polarization purity is needed [3]. However, this increases the device footprint as well as requiring a more complex feeding structure.

The flared slots of the antenna are traditionally described by an exponential curve; however, variations, including multiple exponential curves and elliptical tapers, have also been used [4]–[6]. The Vivaldi acts as a resonant antenna at low frequencies and a traveling wave antenna at high frequencies [7]. The waves travel down the tapered slot, radiating primarily in the endfire direction. Maximum radiation occurs when the separation between the slots is $\lambda/2$, implying the radiator is a discrete region, though it radiates from a slim area. The low-frequency cutoff is generally a function of the maximum slot width. As a traveling wave antenna, the high-frequency cutoff is determined by the practical limitations of the feeding structure [2].

The effects of elliptical pseudoelements on Vivaldi antennas were first explored by Agahi *et al.* [8] in 2011. Two elliptical elements were added inside each of the flares. This was found to extend the impedance bandwidth by improving the matching for low frequencies. Minimal impact on the radiation patterns was reported. This idea was expanded in [7] to show that these directive elements can lead to increased gain. An elliptical element comparable in size to the flares was introduced in the center of the taper. Gain enhancement of greater than 5 dB was achieved at higher frequencies, as well as a decrease in the half-power beamwidth (HPBW). Additionally, the impedance bandwidth remained nearly identical. However, significant sidelobes were introduced at higher frequencies. The E-plane radiation pattern at 20 GHz showed a sidelobe level (SLL) of 2–3 dB.

Fisher [5] designed a Vivaldi with an extremely wide bandwidth of 40:1 operating over 1–40 GHz, but the gain performance leaves something to be desired at the upper end of the band. Past 30 GHz, the gain remained below 8 dB and drops under 4 dB after 36 GHz. Bai *et al.* [6] reported a Vivaldi operating from 4 to 50 GHz with favorable radiation patterns and a peak gain of slightly under 15 dB, though no backlobe levels (BLLs) or cross-polarization levels were shown. Sun *et al.* [9] designed an antipodal Vivaldi operating from 2.8 to 40 GHz with directive radiation characteristics. However, this antenna had less gain than similarly dimensioned Vivaldi antennas. A peak gain of 10.5 dB was achieved with the gain dropping below 7 dB above 33 GHz. Moosazadeh and Kharkovsky [10] presented a compact Vivaldi with a high front-to-back (F-to-B) ratio operating over 3.4–40 GHz.

Manuscript received October 8, 2018; revised February 12, 2019; accepted March 8, 2019. Date of publication March 18, 2019; date of current version July 3, 2019. This work was supported in part by The Ohio State University. *(Corresponding author: Jack Eichenberger.)*

J. Eichenberger and N. Ghalichechian are with the Department of Electrical and Computer Engineering, The Ohio State University, Columbus, OH 43212 USA (e-mail: eichenberger.9@osu.edu; Ghalichechian.1@osu.edu).

E. Yetisir is with SpaceX Corporation, Redmond, WA 98053 USA (e-mail: yetisir.3@osu.edu).

Color versions of one or more of the figures in this paper are available online at http://ieeexplore.ieee.org.

Digital Object Identifier 10.1109/TAP.2019.2906008

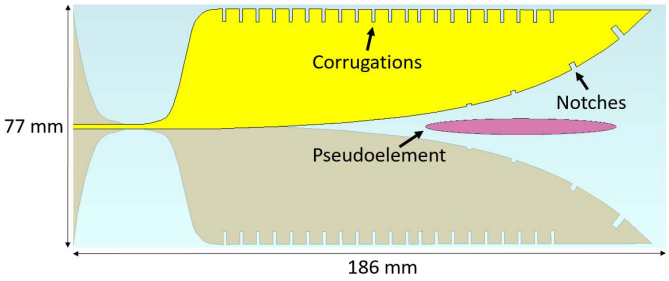

Fig. 1. Vivaldi antenna geometry. Each of the yellow, purple, and brown layers is one of three conductive layers.

A peak gain of 15 dB was achieved. However, some radiation patterns had a broad HPBW of over 60°, while others had high SLLs.

In this paper, we propose a modified antipodal Vivaldi antenna with an elliptical pseudoelement within the tapered slot to improve the directivity and irregularly spaced notches on the slots to decrease sidelobe radiation. Additionally, corrugations are added on the sides of the antenna to reduce the backlobe radiation. To the best of our knowledge, implementing notches that act as radiating elements on the taper of a Vivaldi antenna to reduce sidelobe radiation has not been done before. Preliminary design was presented at [11]; however, this paper includes the final design together with fabrication and measurement results. Theory of operation with discussions on notch and pseudoelement impact is included. Furthermore, depending on any particular application, cross-polarization levels (diagonal plane), time-domain response, and phase center could be of importance. Therefore, these are also discussed in this paper.

Relative to the work reported in the literature, our antenna was able to achieve a higher peak realized gain. We also achieved gains at least 3–4 dB higher for frequencies up to 20 GHz. Our antenna has gain ranging from 10 to 13 dB in the majority of this band, whereas similar Vivaldis have gains in the 6–10 dB range. Above 20 GHz, our gain remains comparable to the state of the art. We were able to realize this performance while maintaining cross-polarization purity of at least 11 dB, low SLLs, and directive beam patterns.

This paper is organized as follows. Section II covers the antenna geometry and design process. Section III discusses the fabrication results followed by the measurement results in Section IV. Comparison between the simulation and measurement results is given in Section IV. Discussions on copolarization and cross-polarization gains (in diagonal plane) and phase center of the antenna are presented in Section V. Moreover, a detailed comparison table is provided. Section VI summarizes and concludes this paper.

II. Antenna Design

A. Exponentially Tapered Slot

Fig. 1 shows the antenna model. The antenna is 0.64 $\lambda_0 \times$ 1.6 λ_0 and 14.7 $\lambda_0 \times$ 35.5 λ_0 at 2.5 and 57 GHz, respectively, where λ_0 is the free space wavelength. The time-domain solver (CST Microwave Studio) is used for all simulations, as it lends itself better to electrically large and UWB structures.

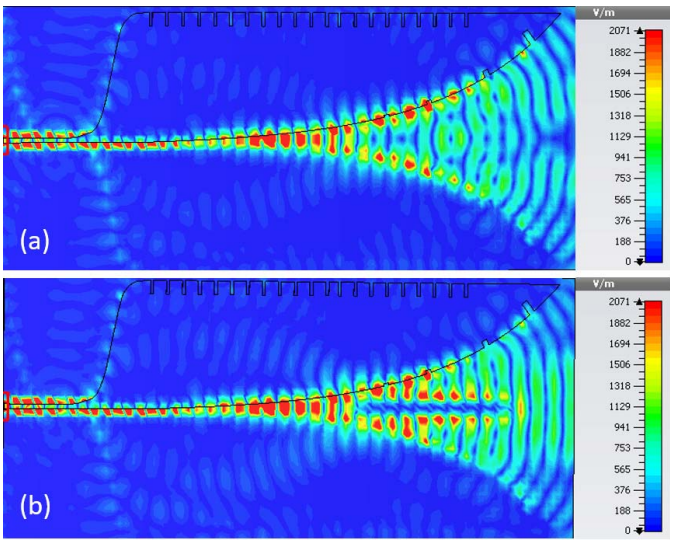

Fig. 2. Wave propagation at 26 GHz along the Vivaldi antenna (a) without and (b) with a pseudoelement.

The simulation has over 93 million mesh elements, and hence, it is time-consuming. RT/duroid 6002 (Rogers corporation) with permittivity of $\varepsilon_r = 2.94$ and $\tan \delta = 0.0012$ is chosen as the substrate. The substrate and conductor thicknesses are 0.508 and 0.018 mm, respectively.

An exponential curve is chosen for the slot. The defining equation is given as

$$y = e^{bx} \tag{1}$$

where b = 0.0269. An exponentially tapered slot is important because it permits for a smooth transition, hence allowing for the traveling wave behavior. Other smooth transitions, such as linear, elliptical, and circular, offer comparable performance. For our design and frequency range, an exponential taper offered slightly smaller dimensions.

B. Pseudoelement

As the antenna reached frequencies above 20 GHz, the SLL increased until the sidelobes became larger than the endfire gain at frequencies above 30 GHz. A directive pseudoelement was added to focus the sidelobe energy into the endfire direction.

The pseudoelement can be seen in Fig. 1 and is an ellipse with major and minor radii of 30 and 2.5 mm, respectively. The pseudoelement shape and dimensions were optimized for antenna performance, namely, to achieve a small SLL. The element had a negligible impact on impedance matching. The length of the major and minor radii did not have a significant effect past a major radius length of 20 mm. Rectangular, triangular, and other shapes were considered, but an ellipse offered the best performance, as it effectively divides the original tapered slot antenna into two tapered apertures. The pseudoelement improves directivity by guiding the wave through the center of the antenna, thereby increasing the endfire gain. We illustrate this concept using the simulation results in Fig. 2. Notice that the electric

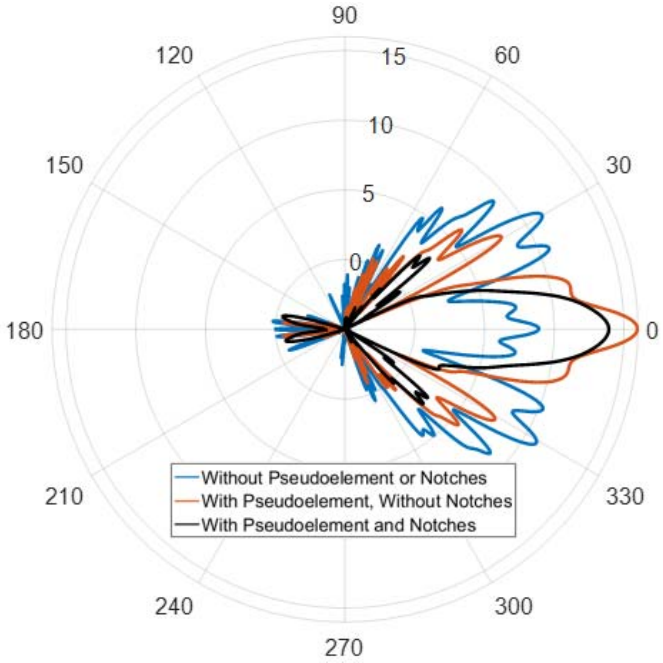

Fig. 3. E-plane radiation pattern (dB) at 32 GHz, showing the effects of the pseudoelement and notches. Patterns shown are the antenna without notches or a pseudoelement (blue curve) with a pseudoelement but without notches (orange curve) and with both a pseudoelement and notches (black curve).

field is more focused in the center when the antenna has a pseudoelement.

Prior to the addition of the pseudoelement, the radiation pattern degraded at >20 GHz due to decreased the endfire gain and increased sidelobes. The endfire gain was effectively increased, but higher than desired SLLs were still present after the addition of the Pseudoelement, as can be seen in Fig. 3. As illustrated, the pseudoelement increased the endfire gain at 32 GHz by 8 dB while reducing the sidelobes by 3 dB. An SLL of 8.5 dB is achieved, but we sought to further reduce this.

C. Notched Tapered Slot

To reduce the sidelobe radiation still present after the addition of the pseudoelement, four notches of 1.5 mm width were added to each flare of the Vivaldi. The notches function by acting as radiating elements focused in the direction of maximum sidelobe gain. This can be understood through the equivalence theorem [12]. Each notch can be approximated as a rectangular aperture on a conductor. The tangential electric field over an aperture is equivalently a radiating magnetic surface current given by

$$\mathbf{M}_s = a_n x \mathbf{E}_t \tag{2}$$

where $\mathbf{M_s}$ is the magnetic surface current, a_n is the unit vector normal to the aperture, and $\mathbf{E_t}$ is the tangential electric field over the aperture.

As it is well known, for any antenna, the far-field pattern is related to its aperture distribution by the Fourier transform,

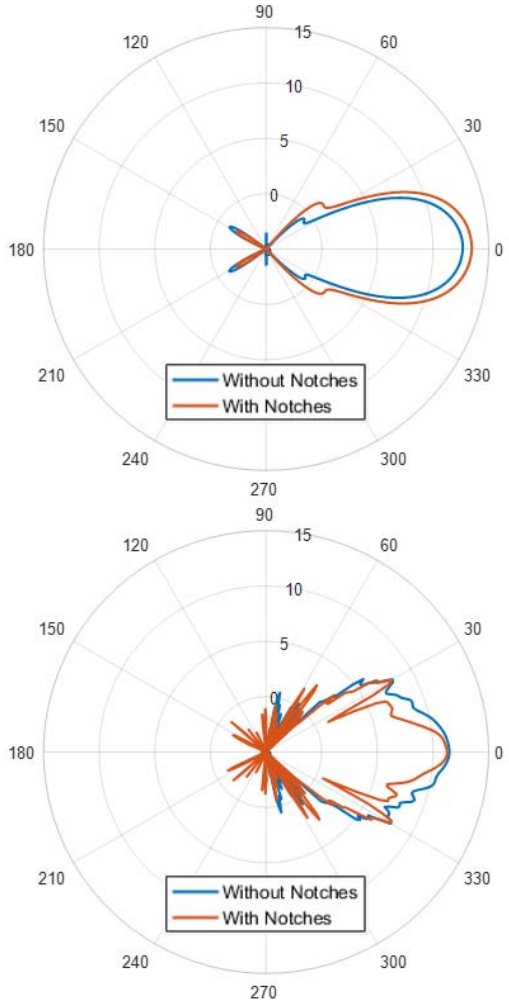

Fig. 4. H-plane radiation patterns (dB) at 10 GHz (top) and 61 GHz (bottom) with and without notches. Notice that outside of 30–60 GHz, the notches are inefficient radiators and have minimal impact on the radiation patterns.

that is

$$E(sin\theta) = \int_{-\infty}^{\infty} E(x_\lambda) e^{j2\pi x_\lambda sin\theta} dx_\lambda \tag{3}$$

$$E(x_\lambda) = \int_{-\infty}^{\infty} E(sin\theta) e^{-j2\pi x_\lambda sin\theta} d(sin\theta) \tag{4}$$

where $E(sin\theta)$ is the far-field distribution, $E(x_\lambda)$ is the aperture distribution, and $x_\lambda = x/\lambda$. For an aperture of width a with a $\lambda/2$ sinusoidal distribution, the resulting far-field pattern is a narrow directive beam with an HPBW of $66°/(a/\lambda)$ and an SLL of -21 dB [13]. In our design, the notches are placed in such a way to destructively interfere with the sidelobes. Due to the requirement of an approximately $\lambda/2$ sinusoidal electric field distribution within the notches for effective radiation, the notches function over roughly 30–60 GHz. Outside of this range, they are inefficient radiators, hence have minimal impact on the far-field pattern. Fig. 4 illustrates this phenomenon. The wavelength at 57 GHz is 3.02 mm, so $\lambda/2$ is 1.51 mm, corresponding to the width of the notches. As the frequency deviates from this range, the notches become less efficient radiators, and hence, this approach is band-limited. The notches' functionality can further be visualized

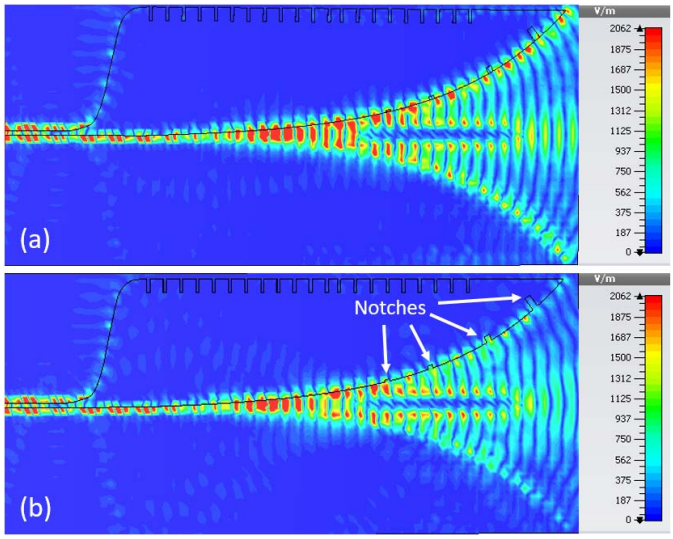

Fig. 5. Electric field distribution at 32 GHz (a) without and (b) with notches.

by observing the electric field distribution. Fig. 5 displays the electric field at 32 GHz with and without notches. Notice the decreased field strength on the flares of the antenna when the notches are implemented, resulting in decrease in far-field SLLs at the given frequency.

The notches allowed us to reduce the sidelobes from 30 to 60 GHz and, thus, significantly extend our high-frequency cutoff from roughly 40 to 57 GHz. Fig. 3 demonstrates an SLL improvement of 3 dB at 32 GHz after the addition of notches. The spacing between the notches as well as the individual depths was optimized for performance. The resulting depths are 0.5, 1.0, 2.0, and 4.0 mm.

D. Corrugations Along the Sides of Antenna

The antenna achieves a maximum gain of 16 dB at 29.8 GHz. At frequencies of higher gain, there is a corresponding larger backlobe. Corrugations on Vivaldis have been used in the past to extend the bandwidths and enhance the gain [10], [14]. The corrugations act as a high-impedance surface at a given frequency, minimizing the radiation leaking backward. The maximum backlobe gain is seen at 26 GHz, so corrugations were added with a spacing corresponding to 0.5λ at 26 GHz and depths corresponding to 0.75λ. This ensures the waves that travel down and back up the corrugations destructively interfere. It is required that the distance to travel down and back up the corrugation is $(n+1/2)\lambda$, where n is an integer and λ is the wavelength of the frequency of interest. We obtained a backlobe gain reduction of 3 dB at 25–27 GHz. While this improves our BLL near the design frequencies, the corrugations can increase the backlobes at other frequencies. The frequencies where backlobes were enhanced (16–18 GHz) already had low levels, so this was not problematic. Fig. 6 shows a 3 dB decrease in the backlobe gain at 26 GHz.

E. Feeding Structure

The designed Vivaldi had an impedance of 166 Ω that we desired to match to a 50 Ω line. A smooth taper from a 50 Ω

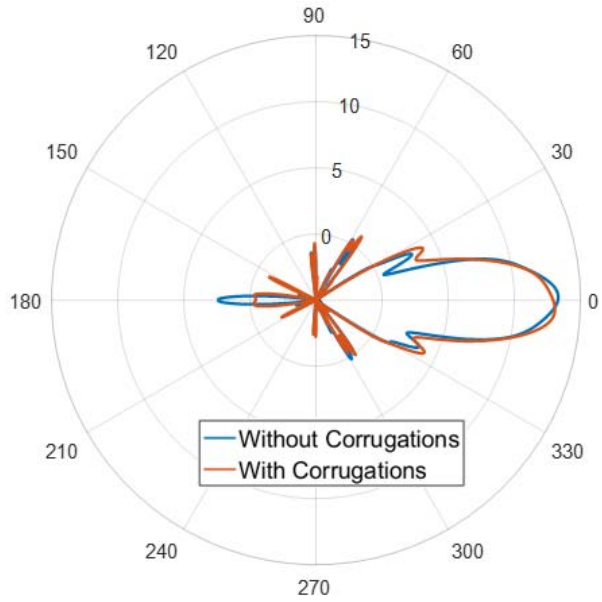

Fig. 6. E-plane radiation pattern (dB) at 26 GHz without (blue curve) and with (orange curve) corrugations.

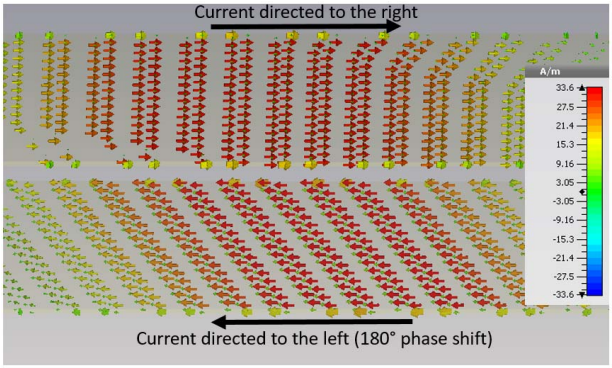

Fig. 7. Surface currents on each of the two striplines. Notice the 180° phase shift between the striplines.

microstripline to parallel striplines was used. The striplines were then smoothly transitioned into the two Vivaldi flares. This is a common approach used by the majority of antipodal Vivaldi antennas in the past. Of the antenna's overall length of 186, 46.5 mm was used for the feeding structure, while the antenna itself made up the other 139.5 mm. In other words, the feed was one-third the length of the antenna. This was found to be the shortest length before the impedance matching was negatively impacted. Similarly, a longer feeding structure did not improve matching. To ensure that we achieved a balanced feed, the surface current on the two parallel striplines was examined and found to be equal in magnitude and opposite in direction. Fig. 7 shows that this condition was met. A complete set of the simulation results for the antenna impedance as well as patterns are presented in Section IV. The simulation results are compared to the measurements.

F. Transient Considerations

A concern with UWB antennas is their susceptibility to dispersion due to the high-frequency content in certain

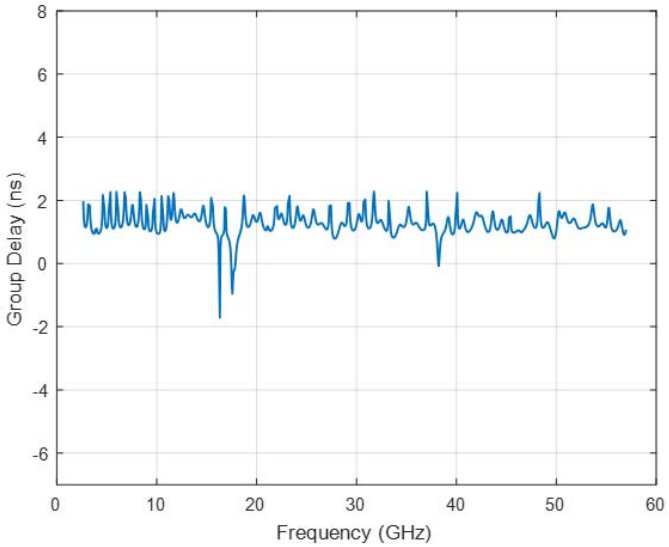

Fig. 8. Simulated antenna group delay as a function of frequency.

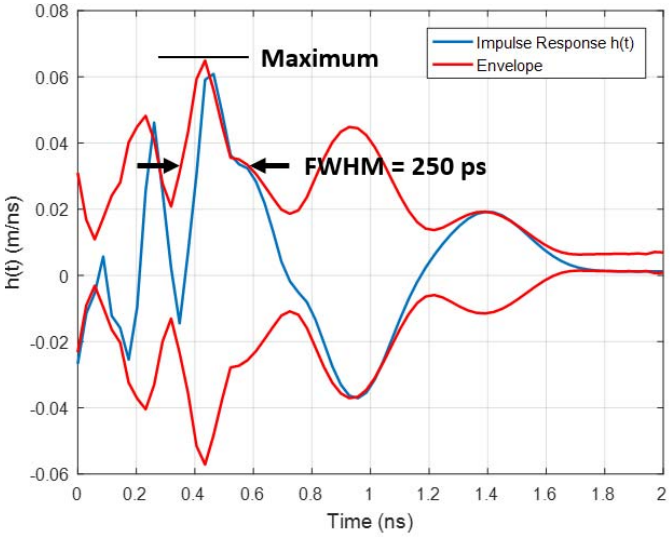

Fig. 9. Antenna time-domain impulse response and envelope.

applications, such as ground-penetrating radar. High levels of dispersion can limit the efficacy of an antenna. The transient behavior of the proposed antenna has been quantified through its ringing behavior and group delay.

Fig. 8 displays the simulated group delay across the band. The antenna has a group delay spanning 4 ns from 2.5 to 57 GHz. The group delay remains below 2 ns for the majority of the band, indicating minimal phase shift within the operating band. Fig. 8 is in line with other Vivaldi antennas operating at similar frequencies [15].

The ringing is caused by energy storage or internal reflections within the antenna. Ringing can be quantified by examining how quickly the impulse response decays relative to the width of its main pulse. The duration of the impulse response envelope should ideally be no more than a few multiples of the width of the main pulse, given by its full-width at half-maximum (FWHM) value [16]. The proposed antenna has an FWHM of 250 ps with an impulse response duration of 1.7 ns, indicating the acceptable ringing performance. Fig. 9 displays the simulated time-domain impulse response and its envelope. This value is in line with similar UWB antennas. For instance, the Vivaldi in [17] had an 85 ps FWHM response. Furthermore, [18] discusses a spiral antenna as well as a Vivaldi antenna with an FWHM roughly 200 and 150 ps, respectively. Both antennas in [18] have response durations of >2 ns, similar to the antenna discussed here.

We note that, as illustrated in Fig. 9, the main pulse is located at 0.45 ns with two additional pulses at 0.9 and 1.4 ns. Depending on the application, these may impose a limitation on the target resolution. Considering free space propagation, a pulse has a travel time of $\Delta t = 2d/c$, where d is the distance from the transmitter to the target and c is the speed of light in vacuum. Rearranging this yields $d = c\Delta t/2$. The main pulse and the pulse at 1.4 ns are separated by 0.95 ns. This translates into a limitaton that objects within 0.14 m of each other cannot be resolved with the proposed antenna. Therefore, the antenna has limitations for certain applications.

III. Fabrication

The antenna was fabricated on an RT/duroid 6002 substrate with three conductive layers. This particular laminate was chosen for several reasons. First, as compared to other laminates, the high-frequency performance up to 40 GHz is favorable. The dielectric constant is stable ($\varepsilon_r = 2.94$ at 8–40 GHz) and losses are low ($\tan\delta = 0.0012$ at 10 GHz). Given the very wide bandwidth nature of our design, the fact that the laminate is intended for operating to at least 40 GHz guaranteed that for approximately two-thirds of the band, it acts as expected. Second, the laminate has a very low thermal coefficient of expansion (CTE = 24 ppm/°C in the Z-direction), which results in higher reliability and better matching with the copper layers. Third, it is suitable for space applications due to low outgassing. Fourth, the fabrication and material costs were reasonable.

The pseudoelement needed to be halfway between the two antipodal Vivaldi layers, so the antenna was split into two 0.254 mm thick substrates. The pseudoelement was fabricated on one layer and then 0.0381 mm thick Rogers 3001 bonding film, $\varepsilon_r = 2.28$, was used to join the layers. This thin layer was taken into account during simulations, as it resulted in the pseudoelement to be slightly off-centered. This reduced our high-frequency cutoff from 59 to 57 GHz due to the degradation of radiation patterns at the end of the band. Conductor thickness was 0.018 mm. Prior to fabrication, minimum line widths were ensured to be large enough for easy manufacturing.

A 1.85 mm end launch connector (model # 1892-04A-5 from Southwest Microwave) was used to feed the microstrip. This connector is rated up to 67 GHz. For 2–40 GHz measurements, a 1.85 mm male to 2.92 mm female adapter (SM3960 from Fairview Microwave) was used. The fabricated prototype is shown in Fig. 10. We note that since the pseudoelement is fabricated in the middle layer, it is not visible in Fig. 10. The measurement setup is shown in Fig. 11. The antenna is encapsulated between two foam slabs in order to ensure that it is completely flat.

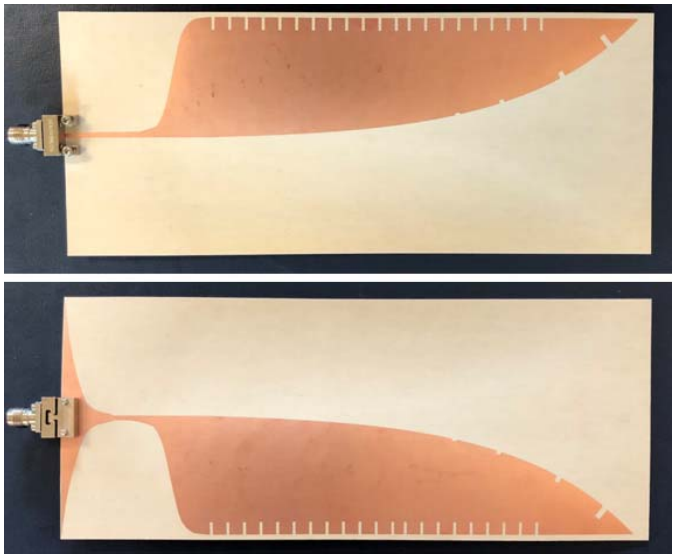

Fig. 10. Top and bottom views of the fabricated antenna. Note that the pseudoelement is not visible because it is in the center layer.

IV. Measurements

Reflection coefficient measurements were done over 1–40 GHz and 40–57 GHz ranges. For frequencies as low as 2.5 GHz, we achieved a VSWR of less than 3 (both simulated and measured), as can be seen in Fig. 12. The majority of the band has a VSWR of less than 2, but there were a few narrow spikes above this in simulations. We achieve excellent agreement between the simulated and measured results. Measured VSWR remains below 2 above 7 GHz. It is implied from Fig. 12 that the antenna can operate above 57 GHz. While it is sufficiently matched above 57 GHz, the radiation pattern degradation is observed above this frequency. An example of this degradation is shown in Fig. 13. Notice the irregularities of the main lobe as well as the SLL approaching zero, as we operate above 57 GHz. Additionally, there are two large sidelobes at 30° to either side of the main beam.

Due to UWB nature of the antenna, the endfire gain measurements were broken into four discrete bands: 2.5–18 GHz, 18–26 GHz, 26–40 GHz, and 40–57 GHz. These bands correspond to the feed horns used in our measurements as well. Radiation patterns were measured simultaneously with the endfire gain with the exception of the 40–57 GHz band. Measurements were performed in the Ohio State ElectroScience Laboratory's Anechoic Chamber. Frequency steps of 5 and 10 MHz were used for 2.5–20 GHz and 20–40 GHz, respectively. A different VNA was used for 20–40 GHz measurements, which is why the step size differs. Due to a limitation of lab equipment and complexity of pattern measurement at the millimeter waveband, only VSWR and endfire gain were measured at 40–57 GHz.

The antenna achieved a gain ranging from 4 dB to a maximum of 16 dB at 29.8 GHz over 2.5–57 GHz. The realized gain remained above 10 dB from 6 to 22 GHz, 13 dB from 25 to 34 GHz, and 10 dB from 34 to 47 GHz. Fig. 14 displays the endfire gain across the entire frequency band.

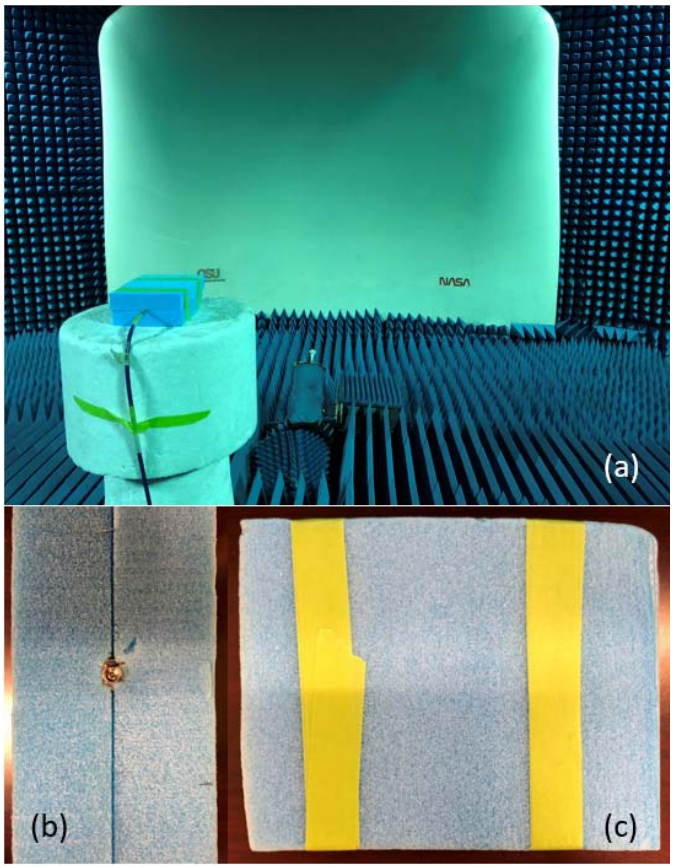

Fig. 11. (a) Antenna under test (AUT), encapsulated in foam, is mounted atop a rotating foam column. The antenna is fed via a horn antenna directed at a parabolic reflector. (b) Back view of the foam capsule with the connector visible. The Vivaldi antenna is between the two foam slabs. (c) Top view of the foam capsule.

Good agreement between simulated and measured results was obtained for both VSWR and endfire gain. Measured gain was within 2.5 dB of the simulated values across all frequencies, with the agreement within 1 dB for the majority of the band.

The proposed antenna achieved high gain across the operational bandwidth, most notably in the first half of the bandwidth, 2.5–20 GHz. The gain performance in this region is higher by 3–4 dB when compared to the similar Vivaldi antennas [6], [10]. The gain remains high in the second half of the band, including a higher peak gain than similar tapered slot antennas [6], [19]. The improvement in the endfire gain can be attributed to the elliptical pseudoelement and notches.

Fig. 15 displays the radiation patterns in the E- and H-planes for five frequencies across the operational band. Both copolarization and cross-polarization levels are shown. A highly directional beam is obtained and confirmed by measurements. For frequencies above 6 GHz, an HPBW of less than 40° in both planes is obtained. Higher frequencies become increasingly directive. For instance, 32 GHz has an HPBW of less than 20°. The radiation patterns display excellent polarization purity. For example, at 8, 20, and 32 GHz, >15 dB of purity is achieved for the main beam and confirmed by measurements.

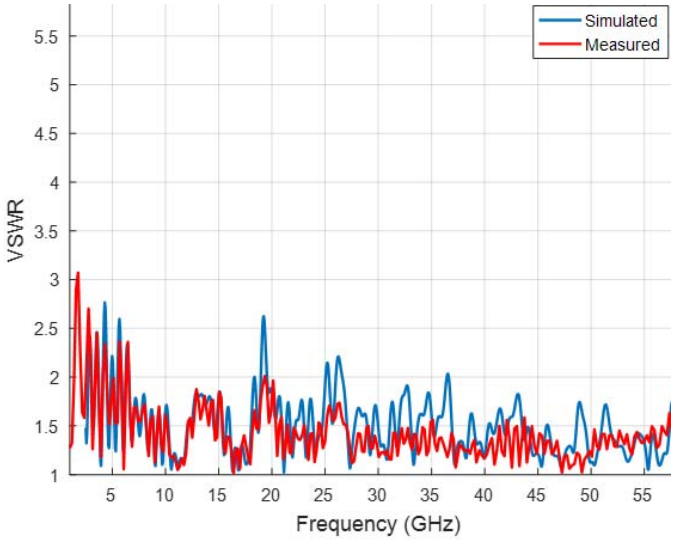

Fig. 12. Simulated (blue curve) and measured (red curve) VSWR from 1 to 57 GHz.

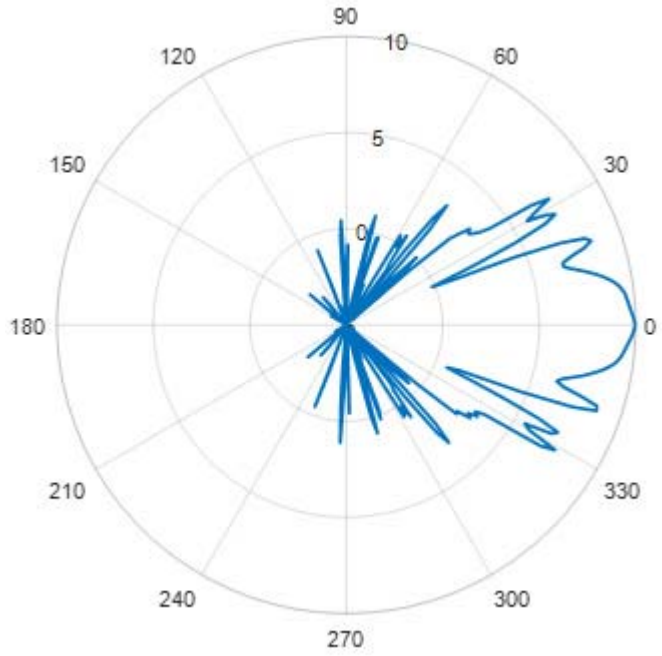

Fig. 13. Simulation results for the H-plane radiation pattern at the 63 GHz displaying pattern degradation. The main lobe of the beam has an irregular shape as well as a 1.5 dB SLL.

As mentioned earlier, for the 40–57 GHz band, only the endfire gain is measured.

V. Discussion

Antipodal Vivaldi antennas are known to have high cross-polarization levels because the E-field is skewed due to the two flares being on opposite sides of the substrate. One method to avoid this problem is to use a thin substrate, as this minimizes the vertical separation between the two flares. We sought to maintain a polarization purity of 10 dB across all operating frequencies. As shown in Fig. 15, 11 dB of polarization purity is achieved for the main beam across the entire band, with most frequencies having polarization purities greater than 15 dB.

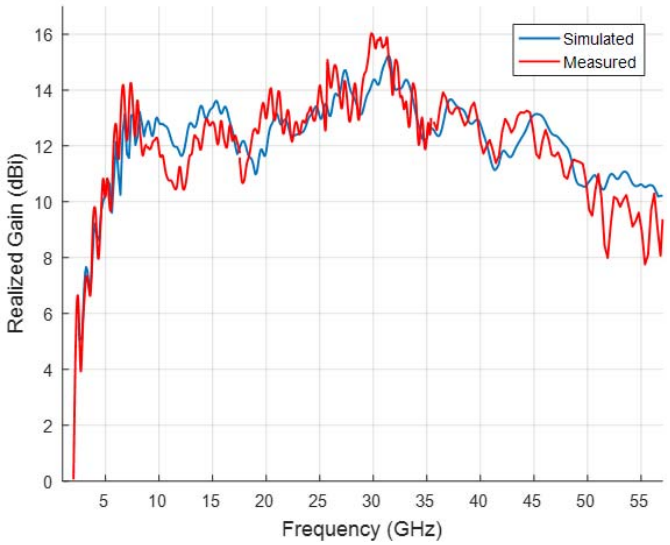

Fig. 14. Simulated (blue curve) and measured (red curve) VSWR from 1 to 57 GHz.

Many works did not report polarization purity [14], [19]. [6] reported the polarization purity of at least 15 dB, while [20] displays purities down to 13 dB. Thus, our antenna has comparable performance in this regard.

Vivaldi antennas occasionally have high cross-polarization levels in the diagonal plane (D-plane), but the proposed antenna does not suffer from this. To illustrate the D-plane purity, a far-field 3-D plot of the cross polarization at 32 GHz is shown in Fig. 16. Performance across the band was similar to the D-plane purity of at least 11 dB. Polarization purity performance can be attributed to the thin substrate, as the two flares of the tapered slot are nearly coplanar. This also contributes to the high-quality radiation patterns since a thin substrate does not support higher order modes at the higher end of the band.

Additionally, the phase center is yet another important parameter for applications, including radar and GNSS. The simulated phase center results are provided in Fig. 17. Overall phase center variations were 70 and 60 mm in the E-Plane and H-Plane, respectively. This corresponds to 11.3 and 13.2 free space wavelengths at 57 GHz.

The proposed antenna offers a high gain of >7.6 dB above 6 GHz with a peak measured gain of 16 dB. Additionally, radiation patterns are favorable in that they are symmetric and directive and have low SLL and BLL. An SLL of 10 dB is achieved for the majority of the band, with the exceptions below 6 GHz due to lower gain and above 45 GHz. These frequencies maintain an SLL of 4 dB. A BLL of at least 10 dB is achieved across the operational band, excluding frequencies below 6 GHz once again due to lower gain.

Table I summarizes the comparison of the proposed antenna to those reported in the literature. Our antenna achieves a larger peak gain as well as an increased bandwidth. To the best of our knowledge, this paper achieves a larger bandwidth than any comparable basic antipodal Vivaldi in the literature. We have also achieved a higher average gain. Our gain is

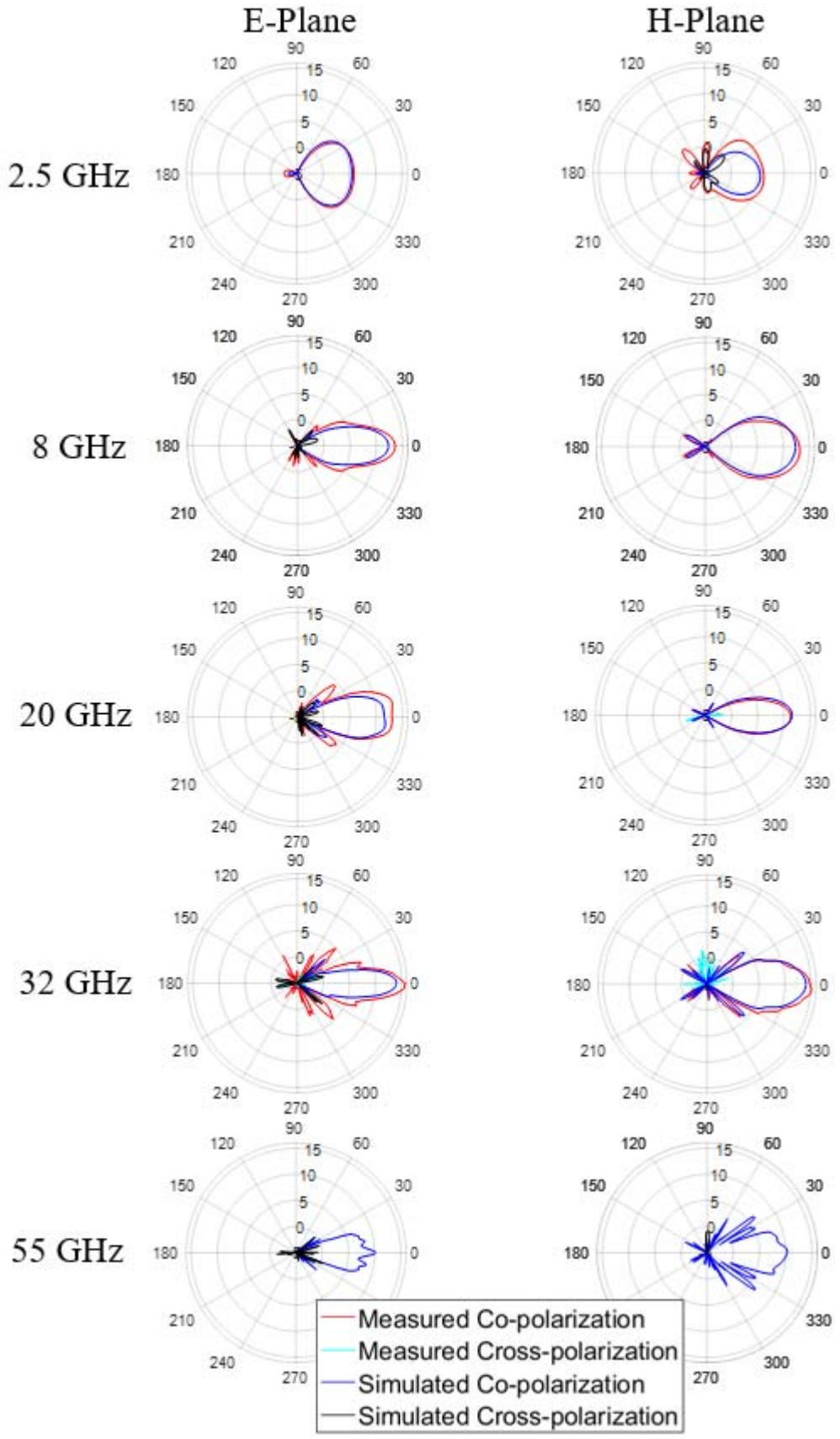

Fig. 15. Measured and simulated radiation patterns in the E-plane and H-plane at 2.5, 8, 20, 32, and 55 GHz.

lower than [21] though that work implemented Teflon layers(lens) surrounding the antenna. This makes fabrication more costly and time-consuming when compared to the simple PCB fabrication.

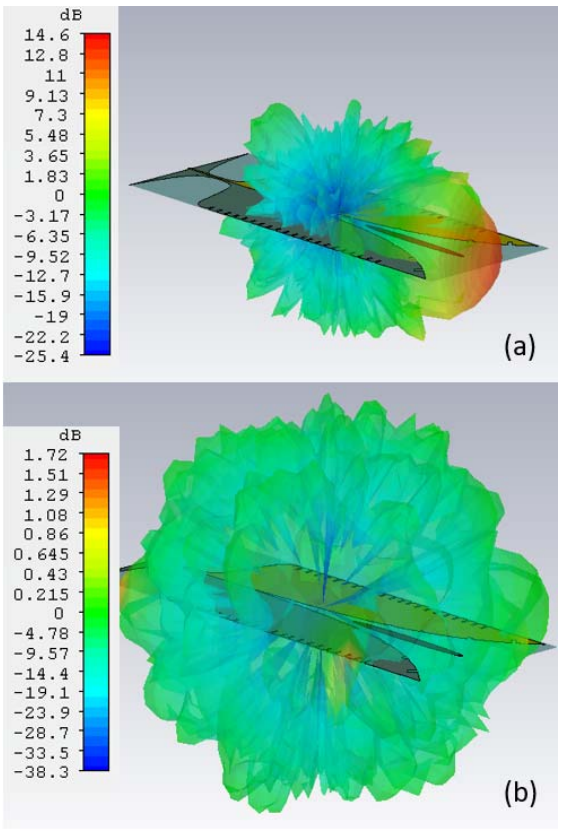

Fig. 16. 3-D far-field plots at 32 GHz of (a) copolarization and (b) cross-polarization. Note that over 14 dB of polarization purity is achieved over the main beam. Cross-polarization levels in this region do not go above 0.5 dB.

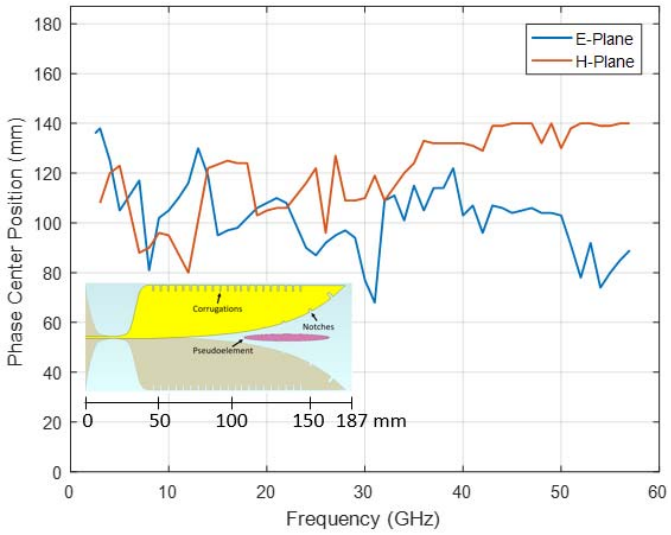

Fig. 17. Simulated phase center for the E- and H-Planes.

We have defined our bandwidth as VSWR < 3, while some works on UWB define bandwidth as VSWR < 2 or 2.5; however, our measured VSWR remains below 2 for the vast majority of the band, besides a few brief spikes. We have also achieved a high peak realized gain and average gain. Our antenna is larger than most references in Table I, but this can be attributed to its higher gain and wider bandwidth. The endfire gain at specific frequencies is also shown for each antenna to better illustrate performance over the operational band.

TABLE I
COMPARISON OF THE PROPOSED VIVALDI ANTENNA

Work	Dimensions (mm^3)	Peak Realized Gain (dB)	Frequency (GHz) → Gain (dB)	Operational Bandwidth (GHz)
[10]	40 × 90 × 0.51	15	4 → 7 20 → 12.5 40 → 14	3.4 - 40
[22]	30 × 55 × 0.51	<14	5 → 6 20 → <12 40 → 13.5	5.0 - 50
[6]	64 × 61 × 0.25	<15	5 → 5 20 → 10 40 → 14.5	4.0 - 50
[23]	96 × 100 × 0.51	12	4 → 7.5 20 → 12	2.1 - 27
[19]	50.8 × 62 × 0.80	10	4 → 5 20 → 9	1.3 - 20
[14]	50 × 62 × 1.52	<11	3 → 6 8 → 10	1.96 - 8.61
[20]	8 × 59 × 0.50	13	25 → >10 40 → 12	25 - 40
[21]	31.6 × 110 × N/A	<21	5 → >6 20 → 17 40 → <21	5.0 - 50
[9]	40 × 100 × 1	10.55	5 → >7 20 → 9.5 40 → >5	2.8 - 40
[5]	20 × 34 × N/A	<12.5	5 → 11 20 → 11.5 40 → 2	1.0 - 40
[4]	151 × 140 × 1.6	N/A	1 → 3 3 → 6 8 → <10	0.73 - 20
This Work	**77 × 186 × 0.55**	**16**	**4 → 10 20 → 12 40 → 14**	**2.5 - 57 (VSWR < 3)**

VI. CONCLUSION

This paper presents a novel design for a UWB Vivaldi antenna with high gain performance across the 2.5–57 GHz band by employing a pseudoelement to enhance directivity, notched flares to reduce SLLs, and corrugations to reduce BLLs. Maximum and minimum gains of 16 and 4 dB are achieved, respectively, across the band. A larger bandwidth (22.8:1) and higher peak gain are presented when compared to similar UWB tapered slot antennas. The antenna offers directive radiation patterns with an HPBW below 40° above 6 GHz, with some frequencies having an HPBW as low as <20° The low profile, high gain, low sidelobe and BLLs, and ultrawide bandwidth make this antenna a good candidate for remote sensing, imaging systems, and defense applications.

REFERENCES

[1] P. J. Gibson, "The Vivaldi aerial," in *Proc. 9th Eur. Microw. Conf.*, Sep. 1979, pp. 101–105.

[2] E. Gazit, "Improved design of the Vivaldi antenna," *Proc. Inst. Electr. Eng. H–Microw., Antennas Propag.*, vol. 135, no. 2, pp. 89–92, Apr. 1988.
[3] J. D. S. Langley, P. S. Hall, and P. Newham, "Novel ultrawide-bandwidth Vivaldi antenna with low crosspolarisation," *Electron. Lett.*, vol. 29, no. 23, pp. 2004–2005, Nov. 1993.
[4] S. A. Abdelbaky and H. F. Hammad, "Modified elliptical antipodal Vivaldi antenna with elliptical tapered slot edge and circular loads," in *Proc. Int. Workshop Antenna Technol., Small Antennas, Innov. Struct., Appl. (iWAT)*, Mar. 2017, pp. 199–202.
[5] J. Fisher, "Design and performance analysis of a 1-40 GHz ultra-wideband antipodal Vivaldi antenna," in *Proc. German Radar Symp. (GRS)*, 2000, pp. 1–5.
[6] J. Bai, S. Shi, and D. W. Prather, "Modified compact antipodal Vivaldi antenna for 4–50-GHz UWB application," *IEEE Trans. Microw. Theory Techn.*, vol. 59, no. 4, pp. 1051–1057, Apr. 2011.
[7] I. T. Nassar and T. M. Weller, "A novel method for improving antipodal Vivaldi antenna performance," *IEEE Trans. Antennas Propag.*, vol. 63, no. 7, pp. 3321–3324, Jul. 2015.
[8] M. H. H. Agahi, H. Abiri, and F. Mohajeri, "Investigation of a new idea for antipodal Vivaldi antenna design," *Int. J. Comput. Elect. Eng.*, vol. 3, pp. 277–281, Jan. 2011.
[9] J. Sun, L. Du, and W. Jiang, "Design of ultra-wideband antipodal Vivaldi antenna for target RCS imaging," in *Proc. IEEE Int. Wireless Symp. (IWS)*, Mar./Apr. 2015, pp. 1–3.
[10] M. Moosazadeh and S. Kharkovsky, "A compact high-gain and front-to-back ratio elliptically tapered antipodal Vivaldi antenna with trapezoid-shaped dielectric lens," *IEEE Antennas Wireless Propag. Lett.*, vol. 15, pp. 552–555, Jul. 2015.
[11] J. Eichenberger, E. Yetisir, and N. Ghalichechian, "Antipodal UWB Vivaldi antenna with pseudoelement and notched flares for 2.5-57 GHz applications," in *Proc. IEEE Int. Symp. Antennas Propag. USNC/URSI Nat. Radio Sci. Meeting*, Jul. 2018, pp. 270–1758.
[12] C. A. Balanis, *Advanced Engineering Electromagnetics*. Hoboken, NJ, USA: Wiley, 2012.
[13] J. D. Kraus and R. J. Marhefka, *Antennas for All Applications*. Boston, MA, USA: McGraw-Hill, 2002.
[14] M. Abbak, M. N. Akinci, M. Çayören, and I. Akduman, "Experimental microwave imaging with a novel corrugated Vivaldi antenna," *IEEE Trans. Antennas Propag.*, vol. 65, no. 6, pp. 3302–3307, Feb. 2017.
[15] Z. Li, X. Kang, J. Su, Q. Guo, Y. L. Yang, and J. Wang, "A wideband end-fire conformal Vivaldi antenna array mounted on a dielectric cone," *Int. J. Antennas Propag.*, vol. 2016, Jun. 2016, Art. no. 9812642.
[16] W. Wiesbeck, G. Adamiuk, and C. Sturm, "Basic properties and design principles of UWB antennas," *Proc. IEEE*, vol. 97, no. 2, pp. 372–385, Feb. 2009.
[17] J. Bourqui, M. Okoniewski, and E. C. Fear, "Balanced antipodal Vivaldi antenna with dielectric director for near-field microwave imaging," *IEEE Trans. Antennas Propag.*, vol. 58, no. 7, pp. 2318–2326, Jul. 2010.
[18] H. Liu, J. Zhao, and M. Sato, "A hybrid dual-polarization GPR system for detection of linear objects," *IEEE Antennas Wireless Propag. Lett.*, vol. 14, pp. 317–320, Oct. 2014.
[19] B. Biswas, R. Ghatak, and D. R. Poddar, "A fern fractal leaf inspired wideband antipodal Vivaldi antenna for microwave imaging system," *IEEE Trans. Antennas Propag.*, vol. 65, no. 11, pp. 6126–6129, Nov. 2017.
[20] J. Puskely, J. Lacik, Z. Raida, and H. Arthaber, "High-gain dielectric-loaded Vivaldi antenna for Ka-band applications," *IEEE Antennas Wireless Propag. Lett.*, vol. 15, pp. 2004–2007, Apr. 2016.
[21] M. Moosazadeh, "High-gain antipodal Vivaldi antenna surrounded by dielectric for wideband applications," *IEEE Trans. Antennas Propag.*, vol. 66, no. 8, pp. 4349–4352, Aug. 2018.
[22] M. Moosazadeh, S. Kharkovsky, J. T. Case, and B. Samali, "Improved radiation characteristics of small antipodal Vivaldi antenna for microwave and millimeter-wave imaging applications," *IEEE Antennas Wireless Propag. Lett.*, vol. 16, pp. 1961–1964, Apr. 2017.
[23] M. Moosazadeh and S. Kharkovsky, "Design of ultra-wideband antipodal Vivaldi antenna for microwave imaging applications," in *Proc. IEEE Int. Conf. Ubiquitous Wireless Broadband (ICUWB)*, Oct. 2015, pp. 1–4.

Jack Eichenberger received the B.S. degree (*magna cum laude*) in electrical engineering from the Rose-Hulman Institute of Technology, Terre Haute, IN, USA, in 2017, where he is currently pursuing the Ph.D. degree under the supervision of N. Ghalichechian.

He is currently a Graduate Student and a Research Assistant with the Department of Electrical and Computer Engineering and the ElectroScience Laboratory, The Ohio State University, Columbus, OH, USA. His current research interests include ultra-wideband antennas, reconfigurable antennas, and metasurfaces in antenna applications.

Dr. Eichenberger was a University Fellow during the 2017–2018 academic year. He was a recipient of the Air Force Research Laboratory SFFP Fellowship for the summer of 2019. He currently serves as a Reviewer for *IET Microwaves, Antennas & Propagation*.

Ersin Yetisir (S'11–M'16) received the B.Sc. degree in electrical and electronics engineering from Bilkent University, Ankara, Turkey, in 2010, and the Ph.D. degree from The Ohio State University, Columbus, OH, USA, in 2015.

From 2010 to 2015, he was a Graduate Research Assistant with the ElectroScience Laboratory (ESL), The Ohio State University, where he was a Post-Doctoral Researcher in 2016. He has worked on wideband and low-profile antenna array and feed-network design for microwave and millimeter-wave frequencies and wideband/multiband antennas with high isolation for MIMO and simultaneous transmit and receive applications. Since 2016, he has been with SpaceX, Redmond, WA, USA, where he has been helping in the design and characterization of low-cost phased array apertures and front-end components and developing calibration methods for satellite and ground terminals.

Dr. Yetisir was a recipient of the Best Student Paper Awards at the 2016 USNC/URSI National Radio Science Meeting (second place) and the 2016 International Workshop on Antenna Technologies (coauthor).

Nima Ghalichechian (S'99–M'08–SM'14) received the Ph.D. degree in electrical engineering from the University of Maryland at College Park, College Park, MD, USA, in 2007.

He developed MEMS electrostatic micromotors supported on microball bearings at the University of Maryland at College Park. From 2007 to 2012, he was a Senior Principal Engineer with the Research Department, FormFactor, Inc., Livermore, CA, USA. During this period, he helped to design and develop MEMS microsprings for advanced probe cards used in testing memory and SoC semiconductor devices. In 2012, he joined The Ohio State University, Columbus, OH, USA, as a Research Scientist, where he is currently an Assistant Professor with the Department of Electrical and Computer Engineering and the ElectroScience Laboratory. As a Principal Investigator, he established several new programs sponsored by NSF, DARPA, and air force research laboratory. From 2016 to 2017, he held a research assistant professor position. He transitioned into an assistant professor position in 2017. He is also a Principal Investigator and the Director of the RF Microsystems Laboratory and advises seven doctoral and two masters' students. His current research interests include phase-change materials, reconfigurable antennas, arrays, ultrawideband antennas, millimeter-wave systems, metasurfaces, 3-D-printed antennas, novel materials, and microfabrication techniques.

Dr. Ghalichechian was a recipient of the 2018 Ohio State University Lumley Research Award, the 2019 National Science Foundation CAREER Award, and the 2019 Air Force Research Laboratory Summer Faculty Fellowship Award.